Miniature Fabry-Perot interferometric sensor for temperature measurement based on photonic crystal fiber*

FU Xing-hu (付兴虎)[1,2]**, **XIE Hai-yang** (谢海洋)[1], **WANG Feng** (王枫)[1,3], **JIANG Peng** (江鹏)[1,3], **FU Guang-wei** (付广伟)[1,2], **and BI Wei-hong** (毕卫红)[1,2]

1. School of Information Science and Engineering, Yanshan University, Qinhuangdao 066004, China

2. The Key Laboratory for Special Fiber and Fiber Sensor of Hebei Province, Qinhuangdao 066004, China

3. College of Mechanical and Electrical Engineering, Hebei Normal University of Science and Technology, Qinhuangdao 066004, China

(Received 10 July 2015)

A novel miniature Fabry-Perot interferometric (FPI) temperature sensor is proposed and demonstrated experimentally. The modal interferometer is fabricated by just splicing a section of photonic crystal fiber (PCF) with a single-mode fiber (SMF). The air holes of the PCF are fully collapsed by the discharge arc during the splicing procedure to enhance the reflection coefficient of the splicing point. The transmission spectra with different temperatures are measured, and the experimental results show that the linear response of 11.12 pm/°C in the range of 30–80 °C is obtained. This sensor has potential applications in temperature measurement field.

Document code: A **Article ID:** 1673-1905(2015)05-0382-4

DOI 10.1007/s11801-015-5131-x

Fiber optic sensors have advantages of small size, fast response, high sensitivity and anti-electromagnetic interference compared with conventional sensors[1-3]. They have been employed in various fields of aerospace applications[4], chemical detection[5], geological survey[6] and many other fields[7,8]. Over the years, several fiber sensors for temperature measurement with different structures or principles have been widely researched, such as Brillouin scattering[9], fiber grating[10-12], Michelson interferometer[13] and other micro-structures[14-16]. Fiber Bragg gratings (FBGs) have a very sharp reflection peak, but they always cost a lot. Long period fiber gratings (LPFGs) have high temperature sensitivity, but they will degrade in high temperature environment. Other sensors mentioned above mostly have a complicated fabrication process. The applications of these sensors are greatly limited by these disadvantages. Therefore, a further research that aims to find a special structure without complexity and high cost is necessary.

In this paper, a miniature Fabry-Perot interferometric (FPI) fiber sensor based on photonic crystal fiber (PCF) is demonstrated. It is fabricated by just splicing a section of PCF with a single-mode fiber (SMF). After the theoretical analysis, an experiment is performed to analyze its temperature sensing properties. Experimental results show that the reflection spectrum shifts to longer wavelength with the increase of temperature. Linear response of 11.12 pm/°C in the temperature range of 30–80 °C is obtained, which indicates that it has both better performance and lower cost compared with the FBGs. Thus, it can be used in different fields of temperature sensing.

The schematic diagram of the proposed FPI sensor is shown in Fig.1(a). During the fabrication process, an end-cleaved PCF is firstly put into the fusion splicer (FITEL S178) and then spliced to an SMF (Corning, SMF-28e). The discharge current and discharge time of the fusion splicer are set to be 84 mA and 500 ms, respectively, so that the air holes in PCF collapse completely to enhance the reflection coefficient. Finally, get out the PCF from the fusion splicer and cleave it to get the desired length. Considering the fringe contrast of the sensor, the length of the sensor should not be too large. The experiment data indicate that the length of 16 mm is the most appropriate. Based on Fresnel reflection, the splicing point and the end of the PCF contacting with the air form reflector 1 (R1) and reflector 2 (R2) of the Fabry-Perot (F-P) cavity, respectively, and their microscope images are shown in Fig.1(b).

As can be seen from Fig.1(a), beam 1 from the light source propagates through the SMF, when it arrives at R1, a part of it (beam 3) is reflected back to the SMF, while the other part (beam 2) transmits into the F-P cavity. Similarly, Fresnel reflection occurs at the moment that beam 2 reaches R2, and then beam 4 and even more

* This work has been supported by the National Natural Science Foundation of China (Nos.61205068 and 61475133), the College Youth Talent Project of Hebei Province (No.BJ2014057), "XinRuiGongCheng" Talent Project and the Excellent Youth Funds for School of Information Science and Engineering inYanshan University (No.2014201).

** E-mail: fuxinghu@ysu.edu.cn

can be stimulated. Finally, reflected light from R1 and R2 interferes with each other in the SMF, and a reflection spectrum with many interference dips can be obtained by utilizing an optical circulator.

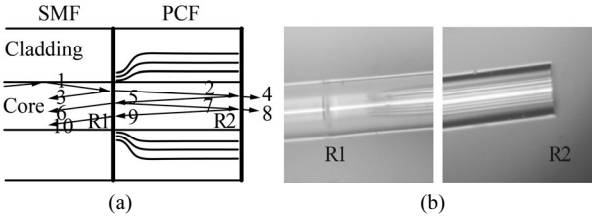

Fig.1 (a) Schematic diagram of the FPI sensor; (b) Microscope images of the two reflection surfaces

In order to explain the reflection spectrum more specifically, the energy of each beam should be considered. According to the Fresnel reflection theory, the reflectivity of R2 is given as[17]

$$R=\left(\frac{n-n_{\mathrm{AIR}}}{n+n_{\mathrm{AIR}}}\right)^2, \tag{1}$$

where the refractive index (RI) of the pure solid-silica core n is 1.458, and n_{AIR}=1 is the RI of the external air. The reflectivity of R2 can be simply calculated, and the reflected energy is less than 4% of that of beam 1. Thus, the energy of beam 10 is far less than 0.16% of that of beam 6. Compared with beams 3 and 6, the total energy of the high-order reflections is very small, which usually can be neglected[18]. Therefore, it can be analyzed just by the simplified two-beam interference model. The optical path difference (OPD) L and reflection intensity I of the FPI sensor can be represented as

$$L=2nl, \tag{2}$$

$$I=I_1+I_2+2\sqrt{I_1I_2}\cos\left(\frac{2\pi L}{\lambda}+\varphi_0\right), \tag{3}$$

where l is the distance between R1 and R2, I_1 and I_2 are the reflected light intensities of the two reflectors respectively, λ is the spatial wavelength, and φ_0 is the initial phase difference of the two reflected light beams. According to Eq.(3), the wavelength dip satisfies the equation of

$$\lambda_m=\frac{2\pi L}{2m\pi-\varphi_0}, \tag{4}$$

which shows the relationship between the wavelength of the mth order dip and the OPD under the condition of the initial phase difference of φ_0. When the FPI sensor is applied to temperature sensing, the OPD will change because the temperature variations make the RI and the length of the sensor changed due to the thermal expansion effect and thermo-optic effect. Thus, the variation of the OPD can be calculated by

$$\Delta L=\Delta n\cdot 2l+2n\cdot\Delta l=2nl\left(\xi+\alpha\right)\Delta T, \tag{5}$$

where Δn is the variation of the RI of the core, Δl is the variation of the distance between R1 and R2, and ξ and α are the thermal-optic coefficient and thermal expansion coefficient of the fiber, respectively. Finally, combining Eqs.(4) and (5), the variation of the wavelength dip is given by

$$\Delta\lambda_m=\frac{4\pi nl\left(\xi+\alpha\right)}{2m\pi-\varphi_0}\Delta T=\lambda_m\left(\xi+\alpha\right)\Delta T. \tag{6}$$

From Eq.(6), we can see that the wavelength dip shift is directly proportional to the increase of the temperature ΔT. Therefore, the temperature of outer environment can be easily detected by observing the change of the transmission spectrum.

In order to investigate the temperature sensing properties of this sensor, a corresponding experiment is conducted. The experimental setup is shown in Fig.2. An amplified spontaneous emission (ASE) optical source ranging from 1 520 nm to 1 610 nm, a three-port C&L band optical circulator and an optical spectrum analyzer (OSA, YOKOGAWA AQ-6317C) are used to record the reflection spectrum. Temperature controlled cabinet (WHL-30B) is used to adjust temperature. The length of the FPI sensor is 16 mm. The PCF used here is SM-10 solid core PCF, which was fabricated by Yangtze Optical Fiber and Cable Joint Stock Limited Company. As shown in the inset of Fig.2, it has a pure-silica core and air holes with micro-structured three-layer hexagonal concentric rings in silica. The core and outer diameters of the PCF are 9.5 μm and 125 μm, respectively. The diameter of the air holes and the spacing distance of the adjacent holes are 2.73 μm and 3.35 μm, respectively. Its thermal expansion coefficient α and thermo-optic coefficient ξ are 5.5×10^{-7} /°C and 6.45×10^{-6} /°C, respectively.

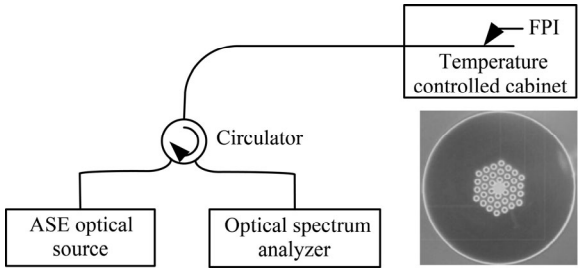

Fig.2 Schematic diagram of experimental setup for temperature measurement (The inset shows the sectional view of the PCF.)

During the whole experiment, the FPI sensor is put on a glass slide with glue to avoid the impacts of fiber bending and strain on temperature measurement result. The reflection spectra are investigated experimentally in the temperature range from 30 °C to 80 °C with an interval of about 10 °C. The temperature is maintained for more than 10 min at each step before the reflection spec-

trum is recorded. The reflection spectra of the FPI sensor with different temperatures are depicted in Fig.3.

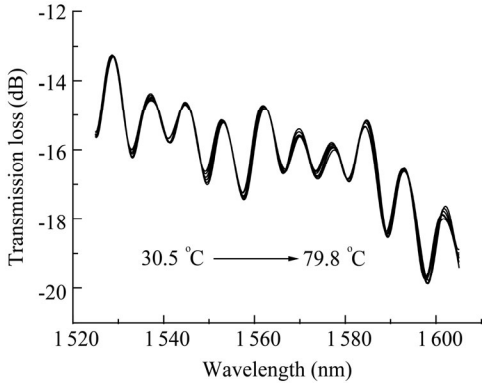

Fig.3 Reflection spectra of the FPI sensor at different temperatures of 30.5 °C, 40.6 °C, 49.2 °C, 59.3 °C, 69.0 °C, 79.8 °C

In order to illustrate the difference of the reflection spectra at different temperatures more directly, four wavelength dips in the spectra are selected as the observation points, which are shown in Fig.4. With the increase of temperature, the wavelengths of the observation points shift toward longer wavelength. Due to the thermal-optic effect and the thermal expansion effect of the fiber, both the RI of the core and the distance between the two reflectors increase as the increase of temperature. According to the analyses above, these two parameters can lead to the variation of the OPD and finally affect the reflection spectrum. Through Eqs.(4) and (6), the wavelengths of the dips with different orders also have direct relationship with the OPD. Therefore, the larger the wavelength of the dip, the higher the temperature sensitivity.

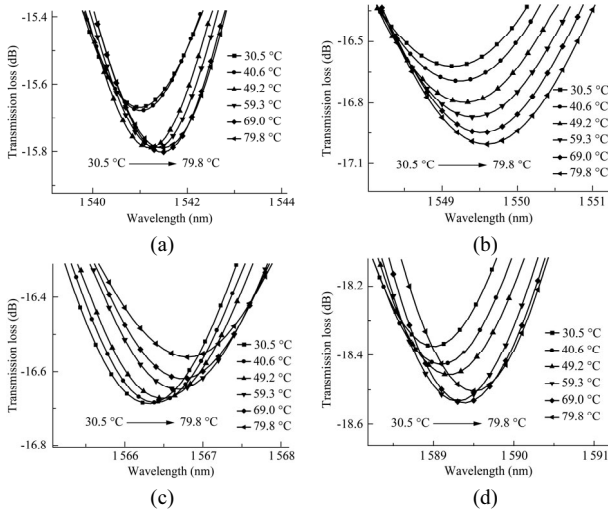

Fig.4 Wavelength shifts at observation points near (a) 1 541 nm, (b) 1 549 nm, (c) 1 566 nm and (d) 1 589 nm with the increase of temperature

Fig.5 shows the relationship between temperature and wavelength for the observation points near 1 541 nm, 1 549 nm, 1 566 nm and 1 589 nm. As shown in Fig.5, there is a good linear relationship between wavelengths of the observation points and temperature, and the temperature sensitivities of the four observation points are 10.78 pm/°C, 10.84 pm/°C, 10.96 pm/°C and 11.12 pm/°C, respectively. Obviously, the temperature sensitivities of the observation points are different, and they are increased with the increase of wavelength dip in the temperature range of 30–80 °C. Moreover, according to Eq.(6), the temperature sensitivity range of the FPI sensor can be calculated, which is 10.64–11.27 pm/°C in the range of 1 520–1 610 nm, and it is close to that of the FBGs[19]. It can be seen that these experimental results agree perfectly with the theoretical data.

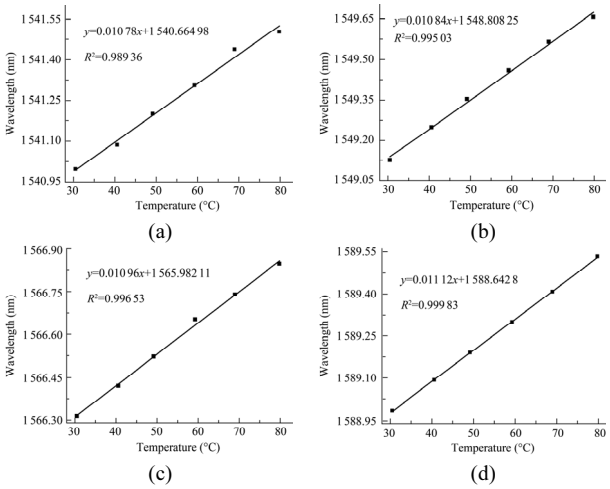

Fig.5 Relationships between temperature and wavelengths of the observation points near (a) 1 541 nm, (b) 1 549 nm, (c) 1 566 nm and (d) 1 589 nm

A novel miniature FPI temperature fiber sensor based on PCF is presented. The sensing mechanism is analyzed accurately, and then its temperature characteristics are experimentally demonstrated. Experimental results indicate that the 16 mm-long sensor can be operated with temperature sensitivity close to that of FBGs within the range of 30–80 °C, and it also has the features of small size, high sensitivity, high stability, simple structure and low cost. Therefore, it is expected to be applied in temperature sensing field.

References

[1] F. F. Pang, W. C. Xiang, H. R. Guo, N. Chen, X. L. Zeng, Z. Y. Chen and T. Y. Wang, Optics Express **16**, 12967 (2008).

[2] L. C. Li, L. Xia, Z. H. Xie and D. M. Liu, Optics Express **20**, 11109 (2012).

[3] GAN Huan-biao, CHEN Zhe, ZHANG Jun, GAN Hong-bo, TANG Jie-yuan, LUO Yun-han, YU Jian-hui, LU Hui-hui and GUANG He-yuan, Journal of Optoelectronics·Laser **26**, 633 (2015). (in Chinese)

[4] H. L. Guo, G. Z. Xiao, N. Mard and J. P. Yao, Journal of Lightwave Technology **31**, 2099 (2013).
[5] R. M. Spearrin, C. S. Goldenstein, J. B. Jeffries and R. K. Hanson, Applied Optics **53**, 1938 (2014).
[6] H. F. Pei, J. H. Yin and W. Jin, Measurement Science and Technology **24**, 095202 (2013).
[7] Z. Y. Chen, Z. M. Dai, N. Chen, S. P. Liu, F. F. Pang, B. Lu and T. Y. Wang, IEEE Photonics Technology Letters **26**, 777 (2014).
[8] Y. Xiao, J. Zhang, X. Cai, S. Z. Tan, J. H. Yu, H. H. Lu, Y. H. Luo, G. Z. Liao, S. P. Li, J. Y. Tang and Z. Chen, Optics Express **22**, 31555 (2014).
[9] X. Liu and X. Y. Bao, Journal of Lightwave Technology **30**, 1053 (2012).
[10] GUO Yong-xing, ZHANG Dong-sheng, ZHOU Zu-de, LI Li-tong and ZHU Fang-dong, Journal of Optoelectronics·Laser **25**, 435 (2014). (in Chinese)
[11] R. Mahakud, J. Kumar, O. Prakash and S. K. Dixit, Applied Optics **52**, 7570 (2013).
[12] Y. Wu, B. C. Yao, A. Q. Zhang, Y. J. Rao, Z. G. Wang, Y. Cheng, Y. Gong, W. L. Zhang, Y. F. Chen and K. S. Chiang, Optics Letters **39**, 1235 (2014).
[13] L. B. Yuan, J. Yang and Z. H. Liu, IEEE Sensors Journal **8**, 1114 (2008).
[14] Q. Wu, J. H. Yuan, C. X. Yu, X. Z. Sang, L. P. Sun, J. Li, T. Guo, B. O. Guan, H. P. Chan, K. S. Chiang, Y. Q. Ma, P. F. Wang, Y. Semenova and G. Farrell, Optics Letters **39**, 6521 (2014).
[15] H. Sun, S. Yang, X. L. Zhang, L. T. Yuan, Z. H. Yang and M. L. Hu, Optics Communications **340**, 39 (2015).
[16] LI Tao, DAI Yu-tang and ZHAO Qian-cheng, Journal of Optoelectronics·Laser **25**, 625 (2014). (in Chinese)
[17] Y. Ma, X. G. Qiao, T. Guo, R. H. Wang, J. Zhang, Y. Y. Weng, Q. Z. Rong, M. L. Hu and Z. Y. Feng, Chinese Optics Letters **10**, 050603 (2012).
[18] M. S. Jiang, Q. S. Li, J. N. Wang, W. G. Yao, Z. W. Jin, Q. M. Sui, Y. H. Ma, J. G. Shi, F. Y. Zhang, L. Jia and W. F. Dong, Optics Express **21**, 3083 (2013).
[19] O. Frazão and J. L. Santos, Journal of Optics A: Pure and Applied Optics **6**, 553 (2004).